Photoluminescence and nonlinear optical properties of triple stranded helicates based metallo-supramolecular architectures

K. Waszkowska, Y. Cheret, A. Zawadzka, A. Korcala, J. Strzelecki, A. El-Ghayoury, A. Migalska-Zalas, B. Sahraoui

Version of Record: https://www.sciencedirect.com/science/article/pii/S0143720820317332
Manuscript_e10f115b0273824ef3a336b460120545

Photoluminescence and Nonlinear Optical Properties of Triple Stranded Helicates Based Metallo-supramolecular Architectures

K. Waszkowska[1,*], Y. Cheret[1], A. Zawadzka[2,3], A. Korcala[2,3], J. Strzelecki[4], A. El-Ghayoury[1], A. Migalska-Zalas[5], B. Sahraoui[1,*]

[1] *University of Angers, MOLTECH-Anjou, UMR CNRS 6200, 2 Bd. Lavoisier, 49045 Angers Cedex 01, France*

[2] *Department of Automatic and Measurement Systems, Institute of Engineering and Technology, Faculty of Physics, Astronomy and Informatics, Nicolaus Copernicus University, Grudziadzka 5, 87-100, Toruń, Poland*

[3] *Centre for Modern Interdisciplinary Technologies, Nicolaus Copernicus University, Wilenska 4, 87-100, Toruń, Poland*

[4] *Department of Biophysics and Medical Physics, Institute of Physics, Faculty of Physics, Astronomy and Informatics, Nicolaus Copernicus University in Toruń, Grudziądzka 5, 87-100, Toruń, Poland*

[5] *Faculty of Science and Technology, Jan Dlugosz University in Czestochowa, Al. Armii Krajowej 13/15, 42201 Czestochowa, Poland*

(*) Corresponding authors: karolina.waszkowska@univ-angers.fr and bouchta.sahraoui@univ-angers.fr

ABSTRACT

The present work is dedicated to the investigation of the linear and nonlinear optical properties of triple stranded metallohelicates in both solid state and in solution. The studied metallohelicates are obtained by a self-assembly process involving three ligands (strands) and "octahedral" like transition metal cations such as iron(II), cobalt(II), nickel(II) and zinc(II), The use of diverse metal cation is motivated by the study of their influence on the linear and

the nonlinear optical properties. The morphology of the thin films of the resulting metallohelicates obtained by spin coating deposition were examined by means of Atomic Force Microscopy (AFM). The properties of these thin films were examined by means of Photoluminescence, Second and Third Harmonic Generation techniques and Z-scan method. The experimental studies allowed us to determine the optical constants. The nonlinear optical susceptibilities of the studied supramolecular metallohelicates were determined by using theoretical models. In this study we have used density functional theory (DFT) to calculate linear and nonlinear optical properties of the investigated molecule. The influence of the interligand $\pi \rightarrow \pi^*$ transmetallic charge-transfer, energy gap and multipole moments at the linear and nonlinear optical properties were discussed.

Keywords: Supramolecular Chemistry, Triple Stranded Metallohelicates, Second Harmonic Generation, Third Harmonic Generation, Z-scan, Nonlinear Absorption, Nonlinear Refractive Index, Atomic Force Microscopy, Luminescence.

INTRODUCTION

Supramolecular chemistry is the chemistry of 21st century. It finds applications in various areas of science: conversion of light by energy transfer [1], conductors of electricity [2], optical sensing [3] and others. Modern supramolecular systems are refined and complex, and some of them are molecular machines modelled on biomolecules such as motor proteins or cancer system cells [4-5]. Therefore, there is an increasingly frequent applications of the achievements of chemistry for the design of new supramolecular systems [6]. Processes of self-assembly of matter have been successfully used to create new materials: supramolecular polymers composed of organic molecules or new porous materials made of small molecules connected by weak noncovalent forces [7-8]. Supramolecular materials play a very important role in medicine. Assemblies are used, for example, to study the interactions of ligands with biomolecules, such as proteins or nucleic acids [9]. The knowledge about these interactions is

currently of great importance in the design of drug delivery [10] like in the treatment of cancer [11]. One of the statutory tasks of supramolecular chemistry is the use of matter to perform calculations at the atomic scale. The storage of the information in supramolecular systems is usually done through the use of molecular switches. Many publications reported data storage in supramolecular systems, such as two-photon induced data storage in supramolecular azopolymers [12] or in thin films formed by supramolecular assembly [13]. Due to their unique properties, supramolecular complexes are promising in nonlinear optics as well as in nanophotonics. Studies of the second order nonlinearity in supramolecular polymers were previously described [14], while some other studies reported the third order optical nonlinearity of metallo-supramolecular complexes based on phthalocyanine [15], fullerenes connected with rotaxanes [16] or of ammonium picrates [17]. Most of the nonlinear optical responses were investigated using Z-scan technique [18-19], although other studies of supramolecular systems were performed for light up-conversion [20]. Note that some low yield luminescent ruthenium(II) triple stranded helicates and their potential applications in medicine have been reported [21].

The main objectives of this work lies on the design and elaboration of new multifunctional supramolecular architectures for NLO applications [22-23]. In this respect, dynamic metal-ligand (M-L) interaction is continuously emerging as a powerful tool for the design and the development of various types of multi-responsive material properties. Such materials can therefore be classified to the kind of stimuli that they respond to, such as thermo-, photo-, chemo-, electro-, mechano-, and offer applications in diverse fields, including biomedicine, nanoelectronics and catalysis [24-27]. Recently a huge interest has been devoted to the preparation of different supramolecular assemblies by the use of suitable ligands that leads to the formation through self-assembly processes to self-assembled metal complexes and/or (metallo)supramolecular networks.

The work reported herein was devoted to study linear, photoluminescent and nonlinear optical properties of some selected metallo-supramolecular triple-stranded helicates and in particular to evaluate the influence of the metal cations used during the self-assembly process such as iron(II), cobalt(II), nickel(II), zinc(II), on such physical properties.

The determination of first and second-order hyperpolarizability of a molecule is often used to understand the affinity between the molecular structure and NLO properties. Therefore we present also the quantum chemical calculation of electronic delocalization through a π-conjugated molecular system. To explain the origin of the NLO phenomena occurring in the investigated supramolecular systems - calculations predicting: HOMO (Highest Occupied Molecular Orbital) and LUMO (Lowest Unoccupied Molecular Orbital), first and second-order hyperpolarizabilities were performed. The calculations of HOMO and LUMO are very important aspects to consider the molecular reactivity.

MATERIALS AND METHOD

Triple stranded helicates

The metal complexes in this research are triple stranded helicates which are resulting from the self-assembly process of three ligands based on iminopyridine fragments and two metal cations, as previously reported [28]. The metal cations being Fe^{2+} (**HelFe**), Co^{2+} (**HelCo**), Ni^{2+} (**HelNi**) and Zn^{2+} (**HelZn**). Fig. 1 presents iminopyridine-based ligand and fig. 2 shows the studied triple stranded metallo-helicates. **Hel-M** guest-host polymeric thin films were prepared using well-known spin coating method from solutions with acetonitrile (ACN) solvent and poly(methyl methacrylate) (PMMA). The concentration of the prepared composition was 10 wt%. Deposition were carried out on strictly cleaned 1 mm glass substrates using spin-coater (Spin200i, POLOS) at speed 2000 rpm.

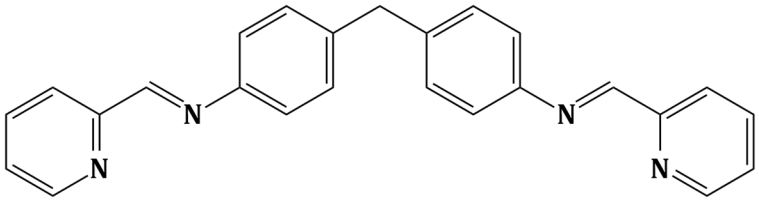

Figure 1: Iminopyridine based ligand used in synthesis of supramolecular triple stranded helicates.

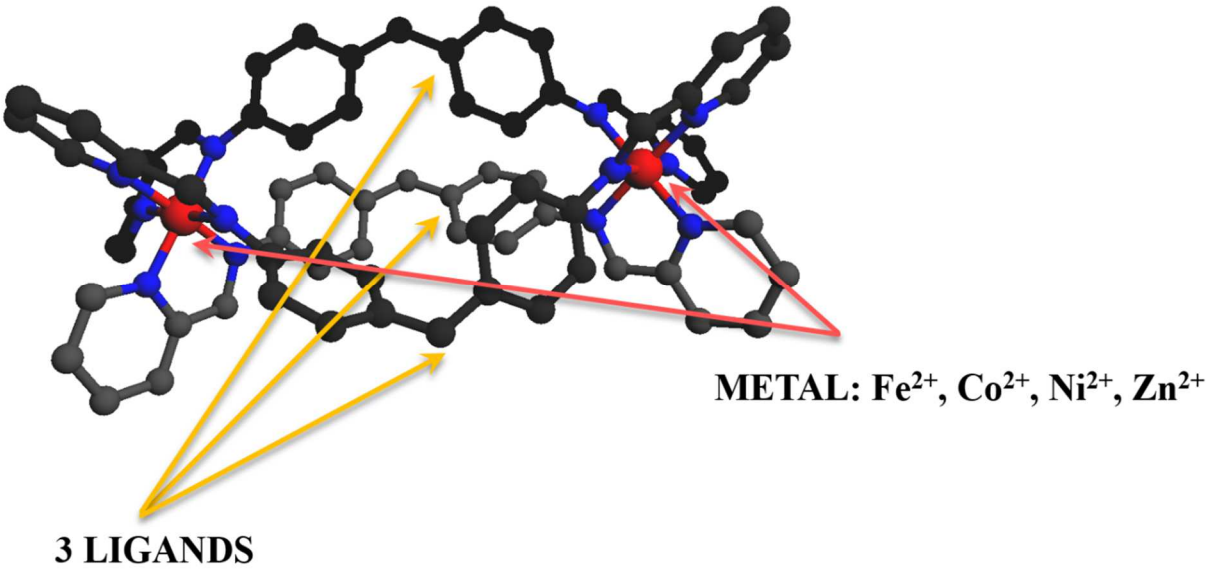

Figure 2: Schematic representation of the studied metallo-supramolecular assemblies.

Characterization techniques of Triple Stranded Helicates

A total of 4 films were collected and their surfaces were analyzed by Bioscope II AFM – Nanoscope V controller (Veeco) [29] with phosphorous n-doped Si cantilever in scanning area 10 × 10 μm^2. UV-Vis spectra of studied thin films were achieved by using UV-1800 spectrometer (Shimadzu) at room temperature. Photoluminescence measurements were recorded on FluoroMax-4 spectrofluorometer (Horiba), while luminescence decay-times were obtained by pulse diode in Single Photon Counting Controller FluoroHub linked to this instrument.

Second- and third harmonic generation measurements were performed on well-known Maker fringe setup [30-32], which is schematically illustrated in fig. 3. Experiment was carried out in transmission manner by rotating sample from -60° to 60° on rotary table. Pulsed Nd:YAG laser (PL2250, Ekspla) generating 1064 nm wavelength was used as a light source and intensities of generated harmonics as a function of rotation angle have been obtained. Measurements were achieved in vertical (P) and horizontal (S) polarized fundamental beam. Interference filter were placed in alignment to cut main wavelength from residual generated harmonics. Parameters of setup used in this experiment are gathered in tab. 1.

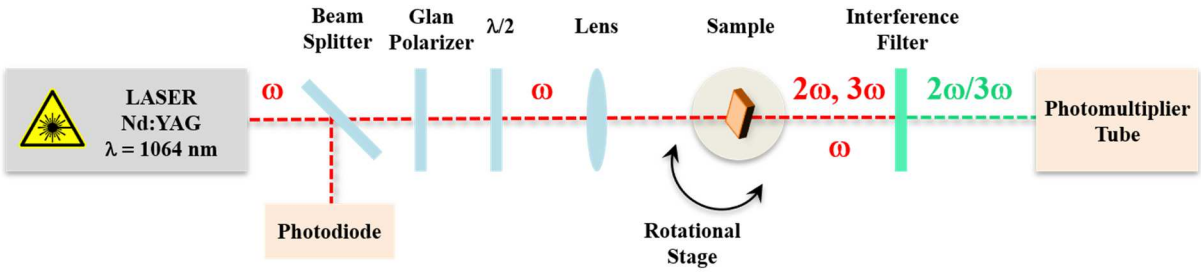

Figure 3: Experimental apparatus for SHG and THG measurements.

SHG measurements were possible by creating macroscopic noncentrosymmetry in studied samples using corona poling technique [33]. Thin films were poled by external electric filed to change the orientation of molecules towards to electric field line. High voltage 6 kV and temperature 100°C, which is close to glass transition temperature T_g of PMMA, were applied for 10 minutes. After this time, the electric field was still applied until the system cooled down. When high voltage is turned off, orientation remains suspended for particular time, depended on the chemical properties of the guest-host system.

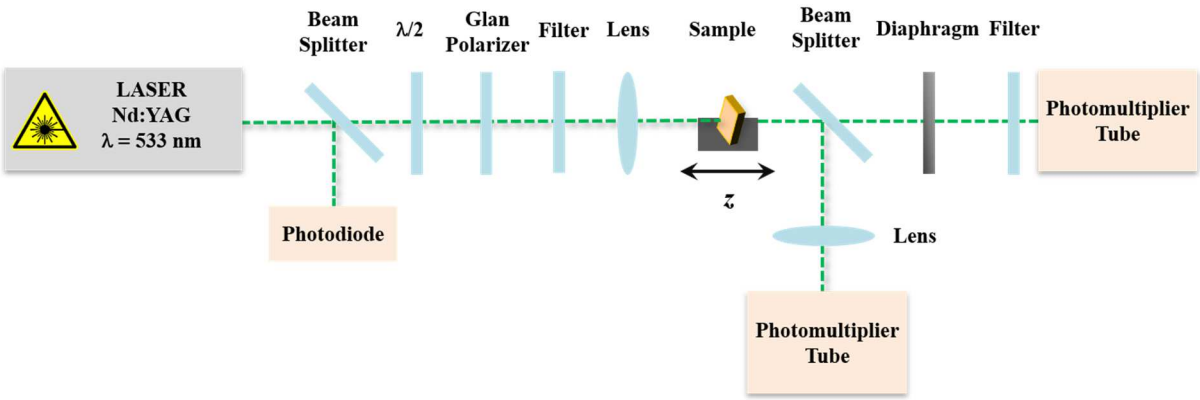

Figure 4: Z-scan experimental setup.

Nonlinear optical properties were investigated by Z-scan technique [30, 34] as well as by using frequency-doubled beam from pulsed Nd:YAG laser in transmission manner (fig. 4). Parameters of alignment used in Z-scan technique are placed in tab. 1. This renowned technique allows us to elucidate nonlinear optical properties, such as nonlinear absorption and nonlinear refractive index, which are measured at the same time. Open aperture Z-scan (OA), where all transmitted light is measured, allows to determine nonlinear absorption, while close aperture Z-scan (CA) involves collecting the small amount of light that is shrouded by the diaphragm (see fig. 4) and allows to determine nonlinear refractive index. We identify two types of nonlinear absorption: saturable absorption (SA) and reverse saturable absorption (RSA), which are determined during measurements in which we receive the transmission in the form of "peak" or "valley", respectively. In the case of close aperture Z-scan, the measured non-linear refractive index can be positive or negative, which corresponds to the "peak-valley" or "valley-peak" configuration, respectively. In this technique samples were investigated in solutions with concentration of about 2.3 mM.

Table 1: Parameters of setup used in SHG/THG and Z-scan measurements

	SHG/THG	***Z-scan***
Laser Wavelength	*1064 nm*	*532 nm*
Laser Energy	*80 μJ*	*0,5–2,0 μJ*
Pulse duration	*30 ps*	*30 ps*
Repetition rate	*10 Hz*	*10 Hz*

Focal length	*25 cm*	*20 cm*
Sample	*thin film*	*liquid*

THEORETICAL MODELS

Comparative model of Lee

Model of Lee is to determine the second-order nonlinear optical susceptibility [35]. Y-cut quartz glass is the most commonly material used as a reference. Second-order nonlinear optical susceptibility $\chi^{(2)}$ of sample with thickness d is calculated from:

$$\chi^{(2)} = \chi^{(2)}_{Quartz}\left(\frac{2}{\pi}\right)\left(\frac{L^{coh}_{Quartz}}{d}\right)\sqrt{\frac{I^{2\omega}}{I^{2\omega}_{Quartz}}} \tag{1}$$

where $I^{2\omega}$ and $I^{2\omega}_{Quartz}$ are the maximum amplitudes of SHG of the investigated material and quartz, respectively, $\chi^{(2)}_{Quartz} = 1.0\ pm \cdot V^{-1}$ [36] is nonlinear optical susceptibility of quartz and $L^{coh}_{Quartz} = 21\mu m$ is the coherent length of the reference material:

$$L^{coh}_{Quartz} = \frac{\lambda_\omega}{4 \cdot |n_{2\omega} - n_\omega|} \tag{2}$$

where λ_ω is the wavelength of the fundamental beam, while $n_{2\omega}$ and n_ω are refractive indexes of the reference material for the fundamental beam and the generated second harmonic, respectively. In the case where the optical absorption of the material is not negligible, the formula (1) includes optical absorption coefficient α:

$$\chi^{(2)} = \chi^{(2)}_{Quartz}\left(\frac{2}{\pi}\right)\left(\frac{L^{coh}_{Quartz}}{d}\right)\sqrt{\frac{I^{2\omega}}{I^{2\omega}_{Quartz}}} \times \left(\frac{\frac{\alpha d}{2}}{1 - exp\left(-\frac{\alpha d}{2}\right)}\right) \tag{3}$$

Comparative model of Kubodera and Kobayashi

The Kubodera-Kobayashi model [37] was used to calculate $\chi^{(3)}$. This model consist in directly comparing the maximum amplitude of the light intensity generated third harmonic

by diagnosed medium with the maximum amplitude of the light intensity obtained in the measurement of 1 mm of silica which is used as a reference material:

$$\chi^{(3)} = \chi^{(3)}_{Silica}\left(\frac{2}{\pi}\right)\left(\frac{L^{coh}_{Silica}}{d}\right)\sqrt{\frac{I^{3\omega}}{I^{3\omega}_{Silica}}} \tag{4}$$

where d is a film thickness, $I^{3\omega}$ and $I^{3\omega}_{Silica}$ are THG intensities of the sample and the silica, respectively, $\chi^{(3)}_{Silica} = 2 \cdot 10^{-22} m^2 \cdot V^{-2}$ [38], $L^{coh}_{Silica} = 6{,}7\mu m$ is the coherent length of silica:

$$L^{coh}_{Silica} = \frac{\lambda_\omega}{6 \cdot |n_{3\omega} - n_\omega|} \tag{5}$$

where λ_ω is the wavelength of the fundamental beam, while $n_{3\omega}$ and n_ω are refractive indexes of the reference material for the fundamental beam and the generated third harmonic, respectively. When the optical absorption is not negligible, the relation (4) includes the linear absorption coefficient α and takes the form:

$$\chi^{(3)} = \chi^{(3)}_{Silica}\left(\frac{2}{\pi}\right)\left(\frac{L^{coh}_{Silica}}{d}\right)\sqrt{\frac{I^{3\omega}}{I^{3\omega}_{Silica}}} \times \left(\frac{\frac{\alpha d}{2}}{1 - exp\left(-\frac{\alpha d}{2}\right)}\right) \tag{6}$$

RESULTS AND DISCUSSION

Surface characterization

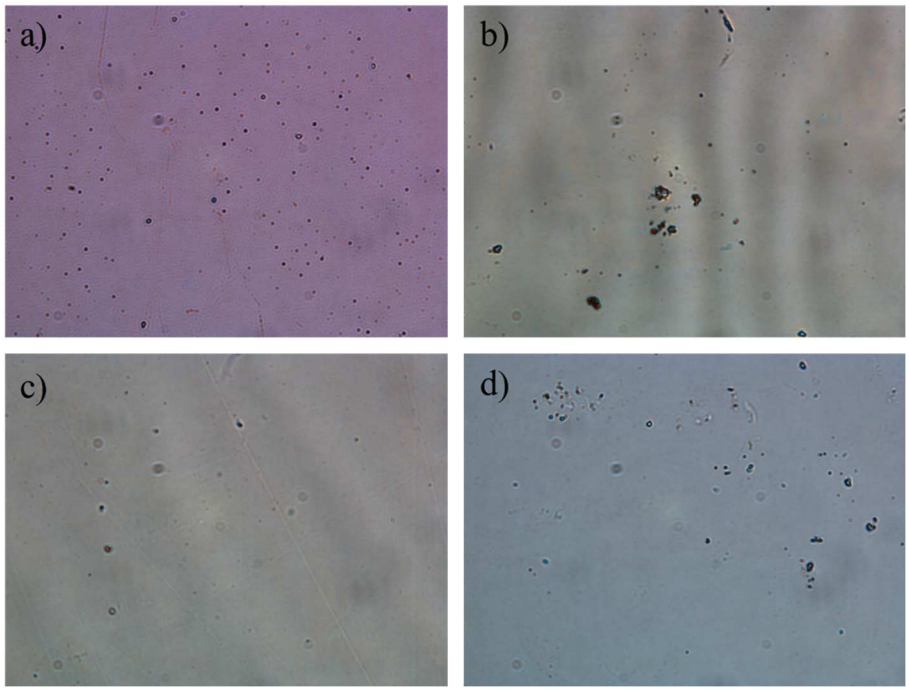

Figure 5: Photographs from optical microscope; a) **HelFe**; b) **HelCo**; c) **HelNi**; d) **HelZn**.

The first order thickness of obtained thin films have been measured using profilometer (Dektak 6M, Veeco). Layers are thinner than 1 micron, and their exact values are given in tab. 2. Afterwards, the photographs of the samples were taken with an optical microscope (fig. 5). In addition to the different colors, some defects in the structure of the layer can also be seen, which were examined in detail using AFM microscope. Typical AFM images analyzed by Gwyddion software are presented in fig. 6. Measurements were carried out in the range

10 μm × 10 μm. It was observed that films are quite homogenous and smooth, although some surface irregularities have been observed. The surface roughness was then measured and calculated. However, the unevenness is not significant - it is at the level of several hundred picometers, in the case of the **HelFe** sample almost one nanometer. This is important when measuring the second and third harmonics to obtain a periodic signal. The obtained values are located in tab. 2.

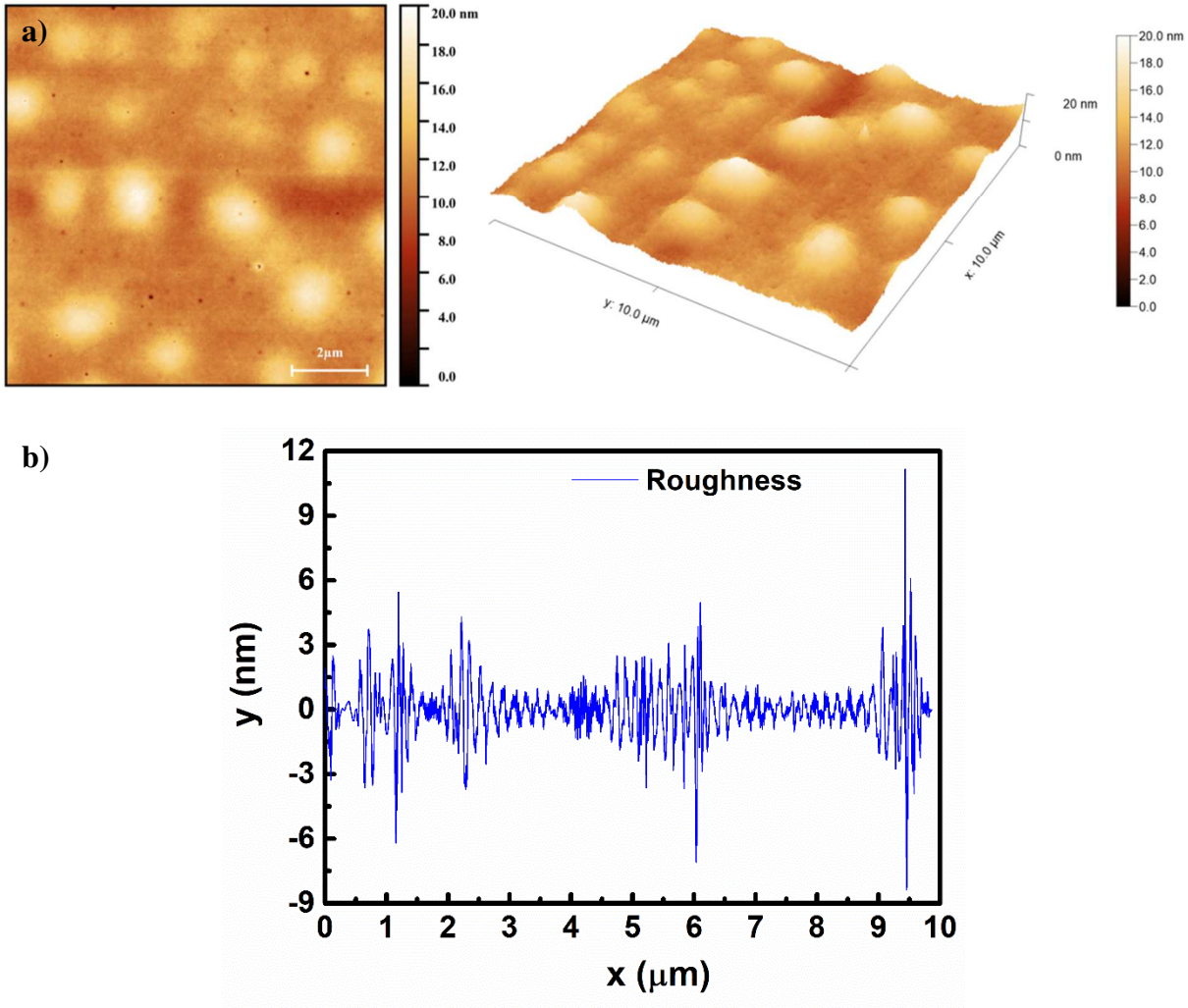

Figure 6: a) Typical 2-D AFM image of triple stranded helicates in the range 10 µm × 10 µm (left) and 3-D view of obtained AFM image (right). b) Typical roughness of studied triple stranded helicates.

Table 2: Thickness and roughness of studied samples.

	Thickness [nm]	**Roughness [nm]**
HelFe	(820 ± 14)	(0,984 ± 0,162)
HelCo	(820 ± 11)	(0,154 ± 0,019)
HelNi	(660 ± 23)	(0,157 ± 0,006)
HelZn	(680 ± 26)	(0,061 ± 0,006)

Absorption spectra

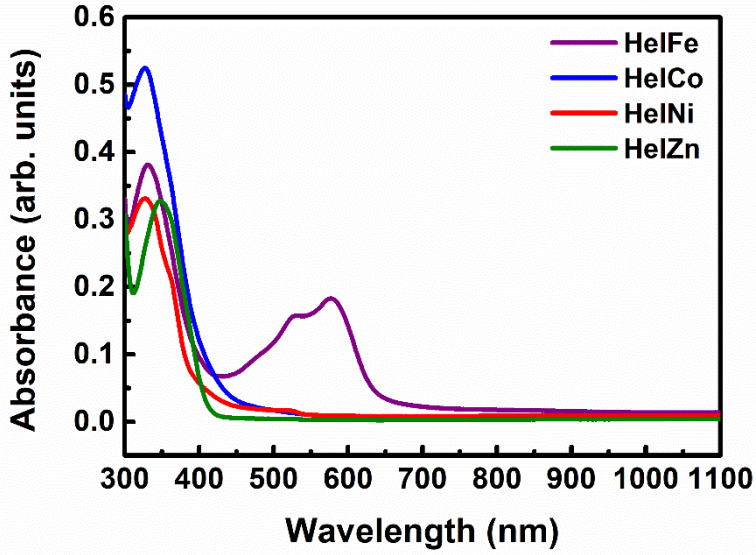

Figure 7: Absorption spectra of studied triple stranded helicates.

Absorption spectra (fig. 7) of the studied thin films were measured by using UV-Visible spectrophotometer in the range 300-1000 nm. Cobalt(II), nickel(II) and zinc(II) exhibit one strong absorption band located at λ_{max} = 355 nm that can be assigned to the $\pi \rightarrow \pi^*$ and $n \rightarrow \pi^*$ interligand charge transfer (^{1}ILCT) transitions. In the case of **HelFe** helicate, in addition to the band located at λ_{max} = 331 nm, the absorption spectrum exhibits a band located in the visible region which is assigned to metal to ligand charge transfer transition (^{3}MLCT) as commonly observed for iron(II) N-heterocyclic ligands [39, 40]. Note that the absorbance at 1064 nm, that constitutes the fundamental wavelength of laser beam at SHG and THG measurements, is negligible. We also noted, that at wavelength corresponding to THG, which is 355 nm, the absorbance is significant which means that simultaneous THG generation is somewhat absorbed. For this reason, the calculations associated with THG experiment have included the absorption coefficient. On the other hand, in case of SHG wavelength, which is 532 nm, absorbance is not negligible for **HelFe** helicate, therefore for this material the calculations was performed by including the absorption coefficient as for THG. Moreover, with the appearance of linear absorption for a wavelength of 532 nm, we should also expect

nonlinear absorption. The exact λ_{max} with absorption coefficients for 532 nm (which corresponds to SHG) and 355 nm (which corresponds to THG) are presented in tab. 3.

Table 3: Absorption peaks and values of absorption coefficients.

	λ_{abs} [nm]	α [10^3 cm^{-1}]	
		532 nm	**355 nm**
HelFe	331, 531, 577	4.49	8.49
HelCo	327	0.35	11.22
HelNi	328	0.50	8.40
HelZn	348	0.12	10.94

Photoluminescence properties

Typical photoluminescence spectra of the studied triple stranded helicates thin films on glass substrates are presented in fig. 8. It was observed that for all samples PL spectra indicate one maximal PL peak in violet wavelength range positioned around 380-410 nm, which are result of ILCT transitions. During excitation at 532 nm and 577 nm sample containing iron(II) **HelFe**, no emission signal was recorded. This is due to the fact that the photoluminescence was carried on thin films containing only 10% of the studied material with the result that both absorption and emission for these compounds are not high intense. 3D photoluminescence spectra shows the intensity for a given emission wavelength as a function of the excitation wavelength. These PL spectra were carried out in the excitation wavelength range 310 nm to 340 nm and emission wavelength range from 350 nm to 500 nm for **HelFe**, **HelCo** and **HelNi**, sample containing zinc(II) was measured in excitation wavelength range from 310 nm to 390 nm and emission wavelength range from 400 nm to 500 nm. As we observed, the strongest enhancement of PL intensity was located near resonant region during excitation by UV light. However it was noted, that PL spectra is determined by asymmetrical shape which is caused by concentration of the samples. By

determining the excitation and emission wavelengths for which the highest intensity occurs, the luminescence decay time was then measured using additional pulse diodes with wavelengths close to excitation wavelengths, which are presented on fig. 9. The lifetime was measured in room temperature, and achieved results were fitted by double-exponential function $y = y_0 + A_0 e^{-t/T_1} + A_1 e^{-t/T_2}$ [41], which implies two time decays T1 and T2. The estimated values of decay times are given in tab. 4. The recorded decay times are very short, first around 1.5-2.0 ns and second around 20-40 ns, which signifies that these samples show fluorescent properties.

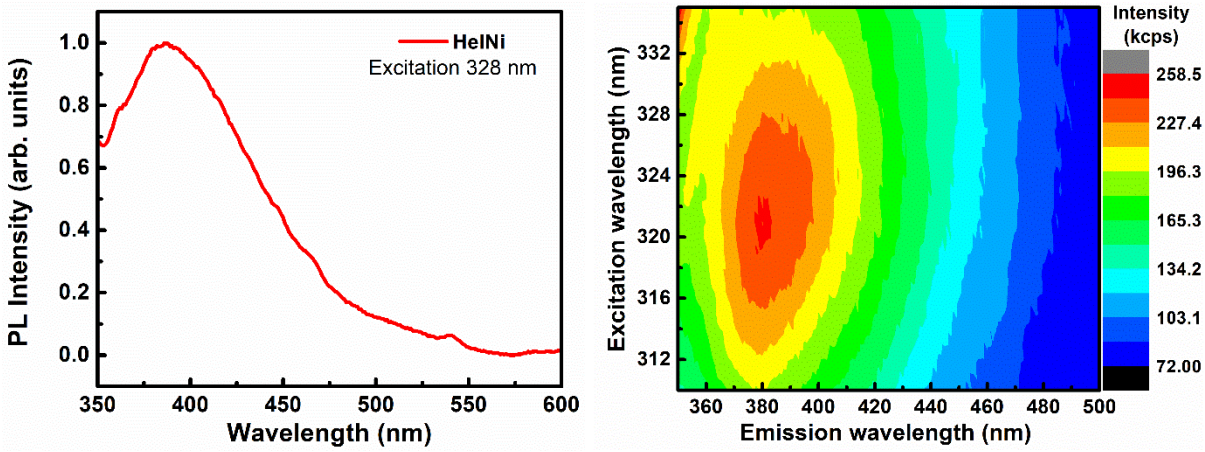

Figure 8: Typical photoluminescence spectra and 3D photoluminescence image of triple stranded helicates.

Table 4: Excitation, emission peaks and luminescence lifetimes of studied thin films.

	$\lambda_{Excitation}$ [nm]	$\lambda_{Emission}$ [nm]	$T1_{Decay}$ [ns]	$T2_{Decay}$ [ns]
HelFe	320	380	(1,562 ± 0,012)	(22,546 ± 0,226)
HelCo	325	400	(1,473 ± 0,011)	(37,872 ± 0,257)
HelNi	328	393	(1,408 ± 0,026)	(23,726 ± 0,242)
HelZn	380	410	(2,005 ± 0,052)	(24,420 ± 0,202)

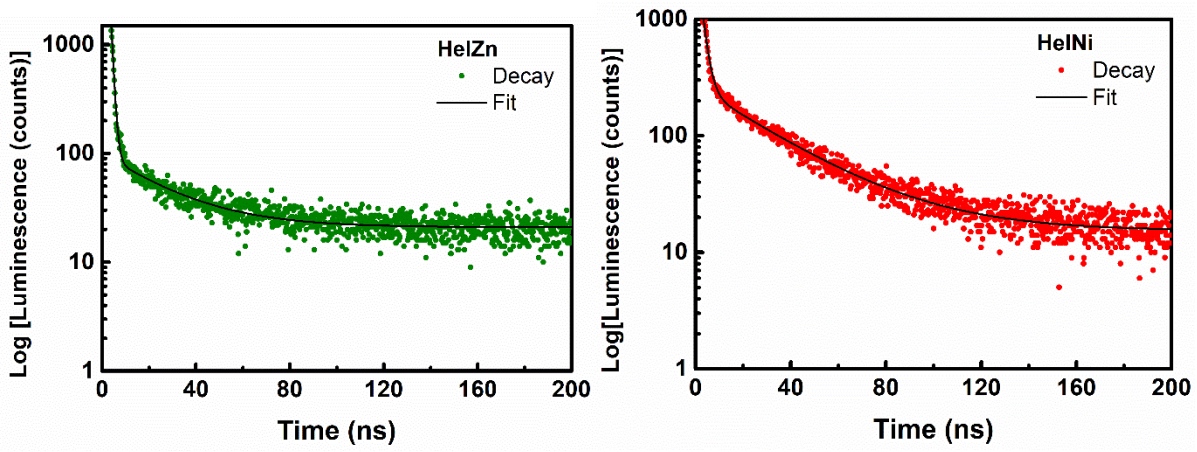

Figure 9: Typical luminescence lifetime decays of studied thin films.

Second and Third Harmonic Generation

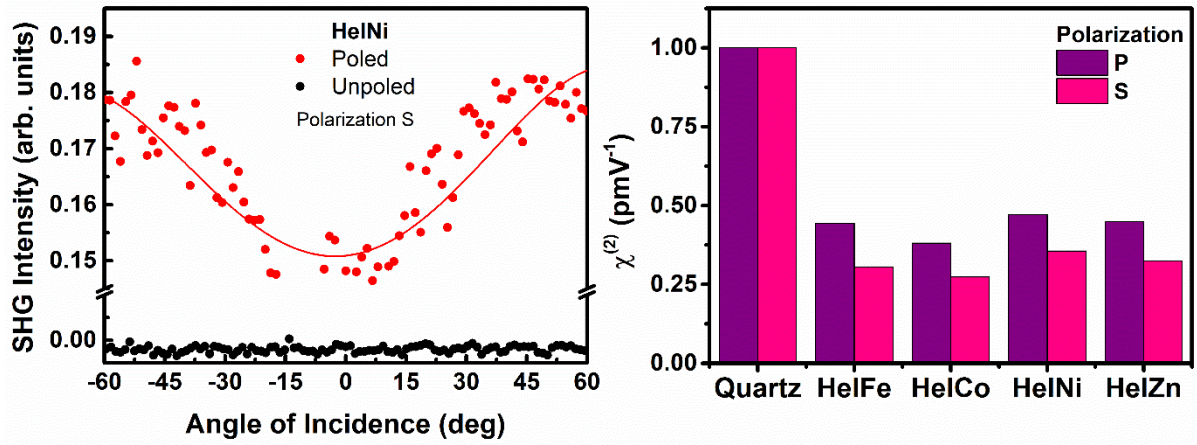

Figure 10: Typical SHG signal of triple stranded helicates before and after corona poling (left); histogram presenting values of second-order nonlinear susceptibility in P- and S-polarized beam (right).

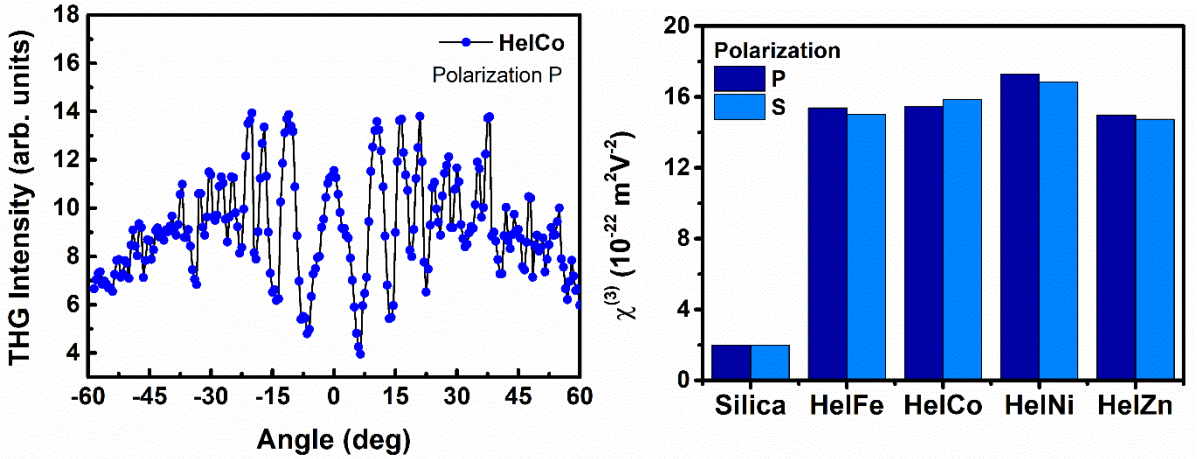

Figure 11: Typical THG intensity as a function of incident angle in P-polarized beam of triple stranded helicates (left); histogram presenting values of third-order nonlinear susceptibility in P- and S-polarized beam (right)

Second and third harmonic generation measurements (fig. 10, 11) were carried out using experimental setup presented in fig. 3. Y-cut quartz plate and silica glass were used as reference materials, respectively. Measurements were performed for vertical (P) and horizontal (S) polarization of fundamental laser beam. On fig. 10a we observe the lack of SHG signal, however after applying the corona poling method, the signal appears. The second order nonlinear optical susceptibilities calculated from the Lee model show that the samples polarize the light in a vertical direction, because the differences between the values depend on the polarization (see tab. 5, fig. 10b). Moreover, outstanding differences were not noticed between the $\chi^{(2)}$ values depending on the metal cation. Basically, THG response is independent from polarization of fundamental beam, however slight differences between calculated values of $\chi^{(3)}$ calculated by using Kubodera-Kobayashi model have been observed (see tab. 5, fig. 11b). This is due to small changes in the laser energy when changing polarization with a half-wave plate. Likewise SHG measurements, there was no significant difference observed for THG with the included metal cation. Nonetheless, the highest values in both experiments have been obtained for triple stranded helicate with nickel cation **HelNi**. Moreover, a comparison between studied triple stranded helicates with previously reported organometallic and supramolecular assemblies has been included. From tab. 5 we can distinctly notice that values of $\chi^{(2)}$ and $\chi^{(3)}$ are approximately higher for triple stranded helicates than the other shown supramolecular and organometallic compounds. It should also be emphasized that these compounds were selected by the method of their preparation and the SHG / THG experimental method.

Table 5: Comparison of total values of second- and third-order nonlinear susceptibility of studied triple stranded helicates thin films with selected compounds in literature.

	$\chi^{(2)}$, pmV^{-1}		$\chi^{(3)}$, 10^{-22} m^{2}V^{-2}	
	P	**S**	**P**	**S**
HelFe	0.444	0.306	15.38	15.02
HelCo	0.381	0.274	15.45	15.85
HelNi	0.472	0.356	17.28	16.84
HelZn	0.449	0.325	14.98	14.74
Benzidofuran-based derivatives S1, S4 [30]	0.12	0.09	5.9	5.1
	0.37	0.13	13.4	13.4
Penta(TMS)C60 [42]	0.19	-	-	9.8
L2Re(CO)$_3$Cl [43]	0.16	0.07	-	8.19

Nonlinear Absorption and Nonlinear Refraction

Analysis of nonlinear absorption and nonlinear refraction have been performed using experimental setup presented in fig. 4. The helicates were dissolved in acetonitrile forming 2.3 mM solution. The measurements were carried out for different laser energies from 0,5 to 2,0 μJ. Only the **HelFe** sample allowed for obtaining nonlinear absorption because it absorbs at 532 nm. Furthermore, **HelFe** sample showed no response in close aperture Z-scan. Achieved responses from OA and CA Z-scan are presented in fig. 11.

Nonlinear absorption coefficient (β) and nonlinear refractive index (n_2) have been calculated from OA and CA graphs using following equations [44-45]:

$$T(z, S = 1) = \sum_{m=0}^{\infty} \frac{\left(-\beta I_0 L_{eff}\right)^m}{\left(1 + \left(\frac{z}{z_0}\right)^2\right)^m (m+1)^{3/2}} \tag{7}$$

$$T(z, S < 1) = 1 - \frac{4\Delta\Phi_0 \frac{z}{z_0}}{\left(\left(\frac{z}{z_0}\right)^2 + 9\right)\left(\left(\frac{z}{z_0}\right)^2 + 1\right)} \tag{8}$$

where: *T(z, S)* is normalized transmittance for OA and CA curves, I_0 – intensity in the center of the beam, z_0 – Rayleigh range, L_{eff} – effective thickness of the sample and is calculated as follows:

$$L_{eff} = \frac{1 - e^{-\alpha_0 L}}{\alpha_0} \tag{9}$$

Moreover $\Delta\Phi_0$ describes nonlinear phase change on the focus and is determined by:

$$\Delta\Phi_0 = \frac{2\pi}{\lambda} n_2 I_0 L_{eff} \tag{10}$$

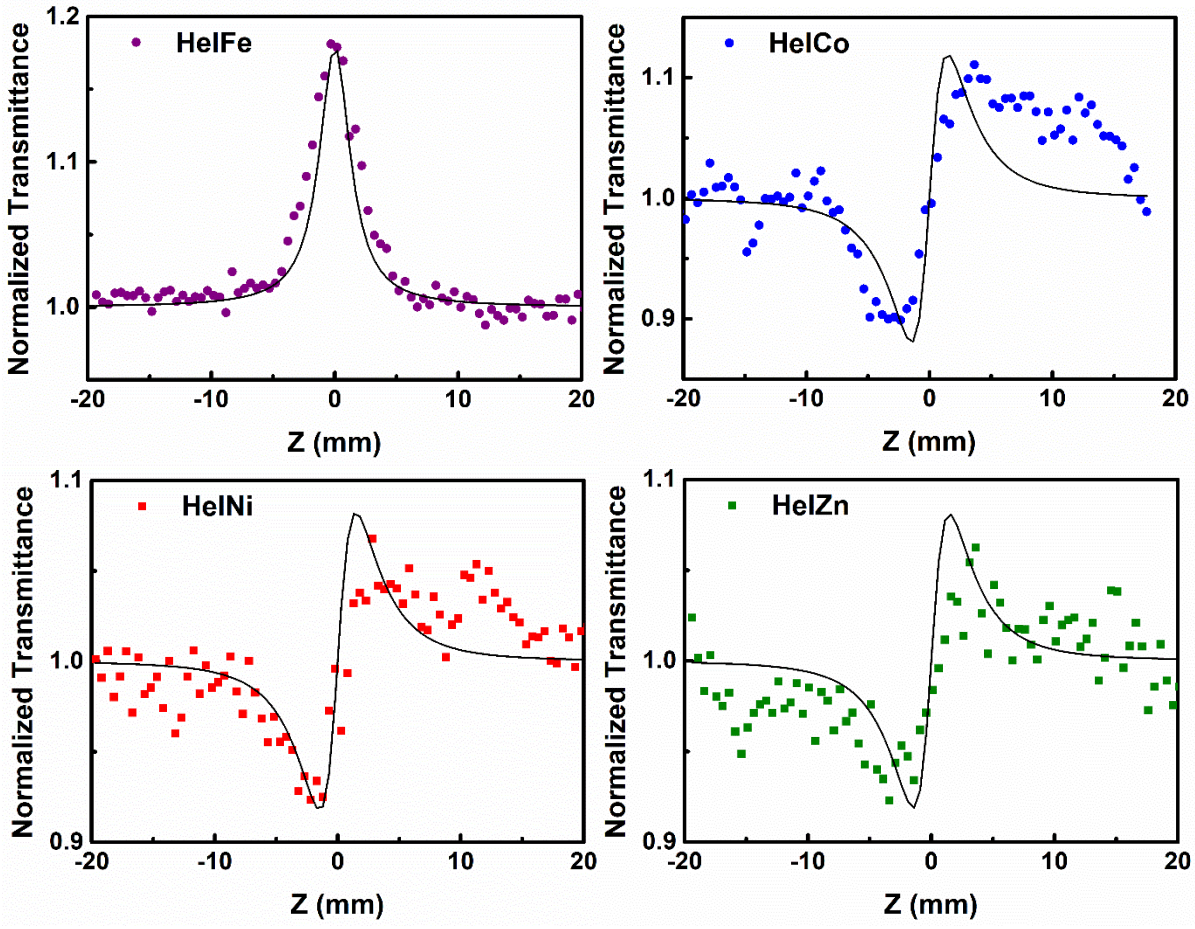

Figure 11: CA Z-scan (left) and OA Z-scan (right) characteristics for triple stranded helicate complexes at concentration 2.3 mM in acetonitrile and laser energy 2.0 μJ.

Values of nonlinear absorption coefficient and nonlinear refractive index are presented in tab. 6. Acetonitrile is characterized by relatively low nonlinearity [46] and its impact on the

obtained results was taken into account during the calculations. Calculated values of $\boldsymbol{\beta}$ and $\boldsymbol{n_2}$, are presented in fig. 12 as a function of laser energy. Calculated values of n_2 correspond to self-focusing behavior. Triple stranded helicate **HelNi** is characterized by the highest total value of refractive index. Moreover, as previously mentioned, absorption coefficient β have been calculated only for **HelFe** complex from saturable absorption response.

Parts of third order nonlinear optical susceptibility have been calculated as follows [47-48]:

$$Re\left(\chi^{(3)}\right) = \frac{4n_0^2\varepsilon_0 c}{3} n_2 \tag{11}$$

$$Im\left(\chi^{(3)}\right) = \frac{n_0^2\varepsilon_0 c\lambda}{3\pi}\beta \tag{12}$$

where c is speed of light in m/s. Obtained NLO parameters are shown in tab. 6. Real part of cubic nonlinear optical susceptibility is for about 3 times higher than $\chi^{(3)}$ obtained by THG technique. We have to take into account that $\chi^{(3)}$ calculated from THG has only electronic contribution, as well as in Z-scan molecular. Besides, aforementioned, measurements were provided for different type of samples - in third harmonic generation experiments were carried out on thin films and in Z-scan technique we used liquid solutions. Furthermore, experiments were carried out in different laser wavelength (1064 nm for THG and 532 nm for Z-scan). However, as in the case of THG studies, the parameters obtained using Z-scan proved to be the best for the **HelNi** sample, although they are not significantly different from the other helicates.

Table 6: Calculated values of NLO refractive index, NLO absorption coefficient, real and imaginary part of third order NLO susceptibility for triple stranded helicates at concentration 2.3 mM in ACN.

	n_2, 10^{-19} m^2W^{-1}	**β, 10^{-12} mW^{-1}**	**Re($\chi^{(3)}$), 10^{-21} m^2V^{-2}**	**Im($\chi^{(3)}$), 10^{-21} m^2V^{-2}**
HelFe	-	-3.52	-	-0.95
HelCo	10.0	-	6.35	-

HelNi	10.15	-	6.45	-
HelZn	9.9	-	6.29	-

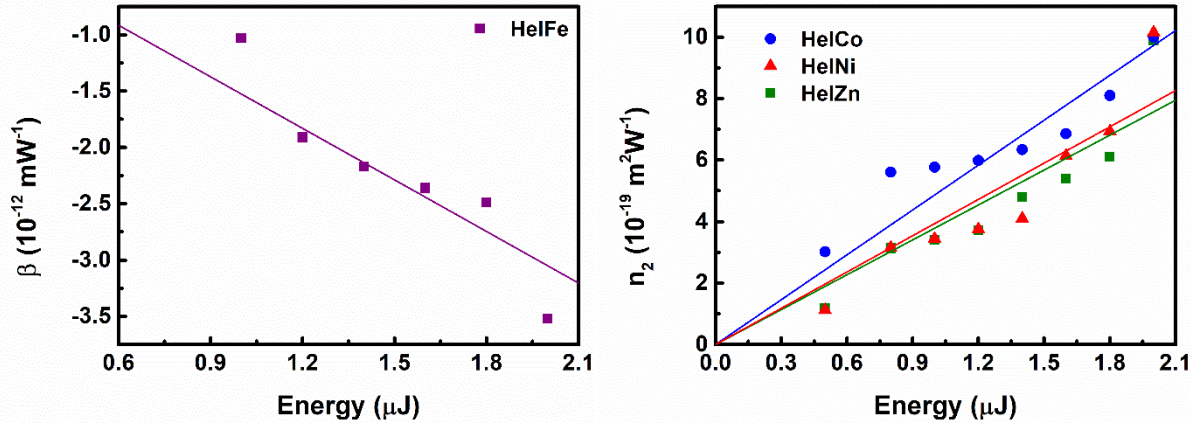

Figure 12: $\boldsymbol{\beta}$ and $\boldsymbol{n_2}$ values as a function of laser energy of **HelFe**, **HelCo**, **HelNi** and **HelZn** complexes in acetonitrile.

Quantum Chemical Calculations

The initial geometrical parameters of the metallohelicates were obtained from Single Crystal X-ray Diffraction refinement data [49]. The optimization of the molecular geometries leading to energy minima was achieved by using density functional dispersion-corrected DFT-D3 theory calculations using B3LYP/6-31+G(d,p) basis set and the UV-vis absorption spectra were computed applying b3lyp/6-31++g(d,p) methodology without dispersion-correction implemented in the GAUSSIAN 09 program package [50] in C1 symmetry. The geometry optimization was performed in gas-phase. Though density functional theory (DFT) is good enough for systems more than 200 atoms, standard semilocal (hybrid) density functional approximations do not describe well the London dispersion energy which is essential for accurate predictions of inter- and intramolecular noncovalent interactions. Therefore dispersion-corrected DFT provides a unique tool for the analysis of complex aromatic systems [51]. The modelled structures were used to calculate HOMO-LUMO energies, frequency-dependent first and second hyperpolarizabilities. It should be mentioned that the empirical dispersion correction mainly affects the geometry of the molecule but is not

effective for the other calculated parameters. The frequency-dependent β(-2ω,ω,ω) and γ(-3ω,ω,ω,ω) parameters at considered ω = 0.04282 a.u. (λ=1064 nm wavelength) were calculated using GAMESS [52] program by B3LYP/lanl2DZ basis set.

Analyzing the values of the position of the absorption maximum λ_{max} calculated theoretically and determined experimentally presented in table 7, one can notice a bathochromic shift of the experimental spectra in relation to the theoretical ones. Which may be related to both the calculation method and the fact that the experimental spectra were made in the solid phase.

Table 7. The computed quantum chemical parameters including: HOMO, LUMO, energy gap $(E_g)_{HOMO–LUMO}$, UV-VIS absorption peak position spectra computed applying b3lyp/6-31++g(d,p) methodology and measured for of studied thin films.

	HOMO [eV]	**LUMO [eV]**	**$(E_g)_{HOMO–LUMO}$ [eV]**	**λ_{abs} exp[nm]**	**λ_{abs} th [nm]**
HelFe	-3.50	-2.18	1.32	331, 531, 577	272
HelCo	-2.82	-2.57	0.25	327	-
HelNi	-3.12	-1.71	1.41	328	280
HelZn	-4.96	-1.02	3.94	348	278

The highest occupied molecular orbital (HOMO) and lowest unoccupied molecular orbital (LUMO) are validity parameters to study the specific movements of electron transfer in molecules (see tab. 7). The HOMO-LUMO gaps of **HelFe, HelCo and HelNi** are significantly smaller than the energy gap value for **HelZn**. A small energy gap suggested that these molecules are relatively more reactive and less stable than **HelZn**. The connection between the electric dipole moments of an organic molecule having donor – acceptor substituent and first order hyperpolarizability is also very important. In the present case, the dipole moments, μ (measured in Debye units) for investigated complexes are very small which is due to the geometry of the molecule. The obtained results, both experimental and theoretical, suggest quite a good second-order nonlinear response (tab. 9). All atoms and molecules (except S-state atoms) have one or more not disappearing permanent multipole

moments. In the case of microcircuits with octahedral symmetry, there is a need to define higher-order multipoles and a hexadecapole system, the moment of which is determined by the fourth-rank tensor. The Table 7 shows the diagonal components of mulipole moments for the tested molecules. With the high octahedral symmetry all other, except hexadecapole moment, mullipole moments should be zero. In this case the also quadrupole moments-second rank tensor (determined by the charge distribution (see Figure 13) have high values for all molecules and can play a crucial role in the obtained high hyperpolarizabilities. The figure 13 shows the charge distribution for **HelZn** resulting from the natural electrical properties of the system from which we can notice a positive and negative regions of the potential. The positive charges lie closer to the metal cationic center (blue region) the potential becomes positive in this region and their influence on the potential is greater while negative charges (orange region) is located at the ends and in the center of the molecule.

It is known that even in symmetrical systems, the process of polarization occurs under the influence of an external electric field, which gives rise to induced dipoles or dipoles of higher order. In the first approximation, the induced dipole moment D^{ind} is proportional to the external electric field E. In our case molecules have an asymmetric charge distribution and then the components of the dipole moment induced in different directions are different. The total moment induced in the system by the E field is the sum of the linear D^{L} moment and the non-linear moments D^{NL} .

$$D_i^{ind} = D_i^L + D_i^{NL} \tag{13}$$

Where: $D_i^N = \alpha_{ij}\vec{E}_j$, $D_i^{NL} = \frac{1}{2}\beta_{ijk}\vec{E}_j\vec{E}_k\frac{1}{6}\gamma_{ijkl}\vec{E}_j\vec{E}_k\vec{E}_l$, α_{ij}linear polarizability, β_{ijk}, $\gamma_{ijkl}\vec{E}_j$ hyperpolarizabilities.

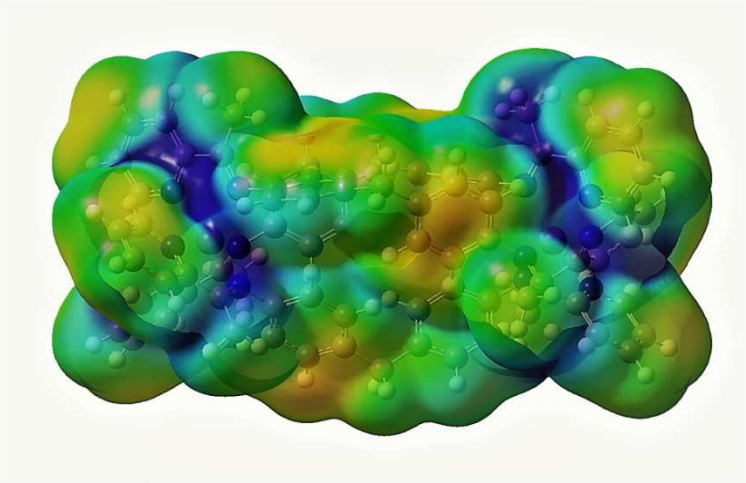

Figure 13: Electrostatic charge distribuition for **HelZn** - positive (blue) and negative (orange) regions. (b3lyp/6-31++g(d,p)).

Table 7: The computed several components of multipole moment (b3lyp/6-31++g(d,p))

HelFe, HelNi, HelZn, HelCo.

	Dipole moment [D]	Quadrupole moment [D·A^2]	Octapole moment [D·A^3]	Hexadecapole moment [D·A^4]
HelFe	X=-0.0018 Y=0.0015 Z=-0.0015	XX= 385.2520 YY= -372.7489 ZZ= -372.7515	XXX=-0.2499 YYY=-64.3741 ZZZ=-48.0822	XXXX=-38918.5639 YYYY=-14408.8966 ZZZZ=-14406.8236
HelNi	X= 0.0010 Y= 0.0007 Z= -0.0005	XX= 395.2342 YY= 369.9974 ZZ= -370.0073	XXX= 0.1302 YYY= -37.8839 ZZZ= 99.7292	XXXX=-38367.2839 YYYY=-14643.4441 ZZZZ=-14642.8189
HelCo	X= -0.0626 Y= 0.1127 Z= -0.3155	XX= 374.4975 YY=-424.3843 ZZ=-426.5068	XXX= -3.6572 YYY=-86.5759 ZZZ= -35.5395	XXXX=45707.3996 YYYY=-15038.9663 ZZZZ=-15080.8357
HelZn	X= 0.0011 Y= 0.0002 Z= -0.0004	XX= 394.2931 YY= -369.7264 ZZ=-369.7332	XXX=0.1446 YYY=-103.6304 ZZZ=-44.5298	XXXX=-38363.2180 YYYY=-14593.7580 ZZZZ=-14592.9995

In this case origin of second-order nonlinear optical properties comes from induced non-centrosymmetricity in the charge density distribution. Table 8 shows the visualized structures of **HelFe**, **HelCo**, **HelNi, HelZn** compounds and depicts the intramolecular transfer of electron density. The maps clearly indicate interligand $\pi \rightarrow \pi^*$ transmetallic charge-transfer

(ITCT). The metal cation moiety has a donor nature and mostly there the HOMO orbital is located. Therefore we can observe the shift of electronic clouds from metal towards the iminopyridine fragment for all the investigated compounds. The first molecular hyperpolarizability β depends not only on the strength of the donor and acceptor groups but also on the nature of the π-conjugated spacer connecting these two groups [53].

The obtained β values for molecules: **HelFe** and **HelZn** have the same order values. A slightly higher value was obtained for **HelZn** (β (-2ω;ω,ω) = 276.785×10^{-30} esu) molecule comparing to **HelFe** (β (-2ω;ω,ω) = 210.078×10^{-30} esu). Urea molecule is the most used reference material for comparison of second order nonlinear optical (NLO) properties of molecular systems. One can observe that the value of first hyperpolarizability β obtained for compound **HelZn** is four orders higher than the one for urea (static first hyperpolarizability for urea molecule β (-2ω;ω,ω) = 30.90 ×10^{-32} esu) [54].

We can easily find a correlation between the parameters characterizing the electronic properties presented in tab.: 7, 8 and the obtained second order hyperpolarizabilities (see tab.9).

Table 8. Frontier molecular orbitals of **HelFe**, **HelCo**, **HelNi, HelZn**, calculated at DFT/B3LYP/6-31G+(d,p) basis set level.

	HOMO	LUMO
HelFe	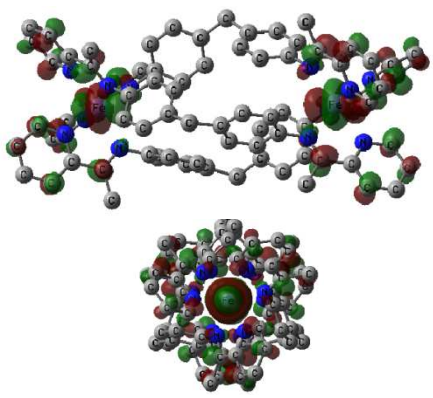	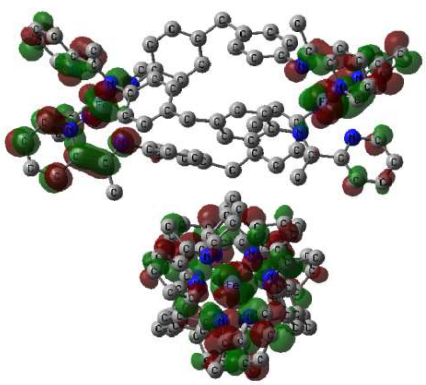

HelCo	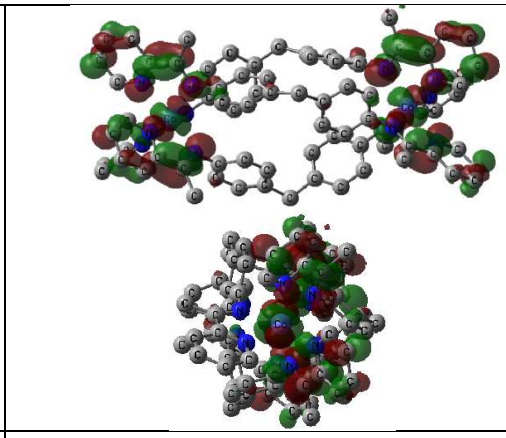	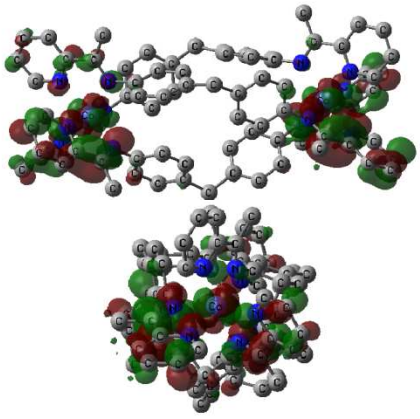
HelNi	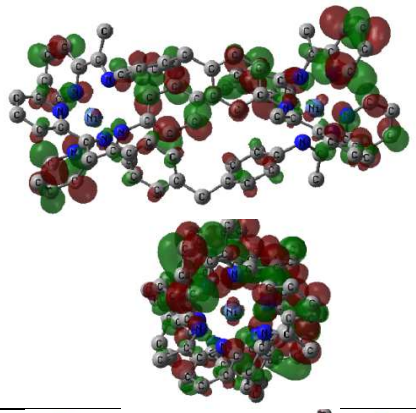	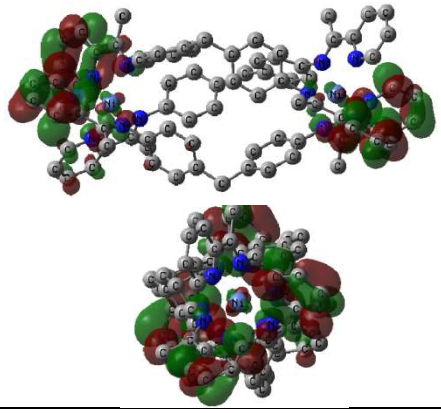
HelZn	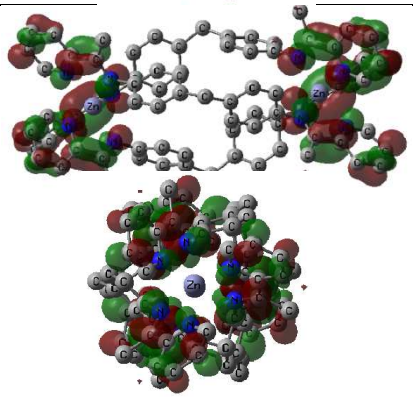	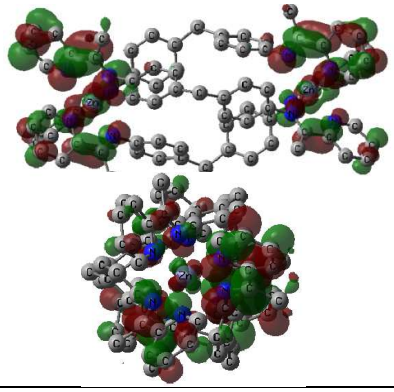

Table 9. Frequency-dependent: $\beta_{tot}(-2\omega;\omega,\omega)$ and $\gamma_{tot}(-3\omega;\omega,\omega,\omega)$ values at ω= 0.042827 a.u., λ=1064 nm, for **HelFe**, **HelZn**, B3LYP/lanl2DZ and comparison with experimental data $\chi^{(2)}$and $\chi^{(3)}$.

	β_{tot} ×10^{-30} esu	$\chi^{(2)}$, pmV^{-1}	γ_{tot}×10^{-36} esu	$\chi^{(3)}$, 10^{-22} m^{2}V^{-2}
HelFe	210.078	0.444	-24167.288	15.38
HelZn	276.785	0.449	-3855.040	14.98

It is known that the relationship of energy gap on the third order nonlinear optical susceptibility is the inverse of the optical break raised to 6th power [55]. As mentioned earlier,

the HOMO-LUMO energy gap for **HelFe** is smallest than for **HelZn** hence the highest value of the second-order hyperpolarizability for **HelFe** is obtained. Decreasing the value of the energy gap increases the charge transfer within the molecule. As you can see from the tab. 9 the second order hyperpolarizability of compound **HelFe** (γ=24167.288×10^{-36} esu) is one order higher than for **HelZn** (γ=3855.040×10^{-36} esu). We also compared our hyperpolarizabilities γ values with reported by Leupacher et al. [56] of methylene blue (γ=32.00×10^{-36} esu) employing THG measurements and the value of γ for **HelFe** is three order higher. The calculated theoretical values of β and γ were found to be in good agreement with the experimental findings.

CONCLUSIONS

Triple stranded helicates: **HelFe**, **HelCo**, **HelNi** and **HelZn** were synthesized and their corresponding thin films were prepared successfully using well-known spin-coating technique. AFM analysis have shown that the obtained thin films are relatively smooth and homogeneous, as demonstrated by the studies of the surface roughness. UV-Visible absorption spectra of the studied complexes showed that their absorption has a large impact on the NLO response. Moreover, in spectroscopic studies ultraviolet emission was observed from photoluminescence studies, and the luminescence decay time is relatively fast, indicating fluorescence like emission.

NLO response of the studied metallo-supramolecular triple stranded helicates have been performed using SHG and THG Maker fringe method and Z-scan technique. The highest quadratic and cubic nonlinear optical susceptibilities have been found for helicate containing nickel metal cations **HelNi**, even if these values for the other samples are not significantly different from each other. For Z-scan studies, only the **HelFe** complex exhibit nonlinear absorption, however, the NLO refraction for this sample has not been obtained. Finally, the

highest value of NLO refractive index have been found for complex **HelNi**, which is consistent with THG results. The theoretically evaluated energy gap of the compounds showing the high rate of electron transfer from the ground to the excited state. However, a significant reduction in the energy gap in the molecule investigated compounds causes a large increase in third-order nonlinear properties. The interligand $\pi \rightarrow \pi^*$ transmetallic charge-transfer (ITCT) supports noncentrosymmetric charge density distribution resulting in the molecules possessing second order NLO properties.

The NLO properties obtained for the metallo-supramolecular triple stranded helicates, indicate that these assemblies can be promising candidates to be used in photonics and nonlinear optical devices applications.

ACKNOWLEDGEMENTS

This research was supported by the European Cooperation in Science and Technology through COST Action MP1403 Nanoscale Quantum Optics. Research in this paper were done using Interdisciplinary Centre for Modern Technologies facilities, NCU, Torun, Poland.

Calculations have been carried out in Wroclaw Centre for Networking and Supercomputing (http://www.wcss.pl), grant № 282.

REFERENCES

[1] T. Hasobe, Supramolecular nanoarchitectures for light energy conversion, Phys. Chem. Chem. Phys., 12: 44-57, 2010.

[2] Puigmartí-Luis, J., Laukhin, V., Pérez del Pino, Á., Vidal-Gancedo, J., Rovira, C., Laukhina, E. and Amabilino, David B., Supramolecular Conducting Nanowires from Organogels, Angewandte Chemie International Edition, 46: 238–241, 2007.

[3] I. V. Kolesnichenko, E. V. Anslyn, Practical applications of supramolecular chemistry, Chem. Soc. Rev., 46, 2385, 2017.

[4] H. Qin, Ch. Zhao, Y. Sun, J. Ren, X. Qu, Metallo-supramolecular Complexes Enantioselectively Eradicate Cancer Stem Cells in Vivo, J. Am. Chem. Soc. 139, 16201-16209, 2017.

[5] H. Wang, Z. Feng, D. Wu, K. J. Fritzsching, M. Rigney, J. Zhou, Y. Jiang, K. Schmidt-Rohr, B. Xu,Enzyme-Regulated Supramolecular Assemblies of Cholesterol Conjugates against Drug-Resistant Ovarian Cancer Cells, J. Am. Chem. Soc., 138, 34, 10758-10761, 2016.

[6] F. D'Souza, P. M. Smith, S. Gadde, A. L. McCarty, M. J. Kullman, M. E. Zandler, M. Itou, Y. Araki, O. Ito, Supramolecular Triads Formed by Axial Coordination of Fullerene to Covalently Linked Zinc Porphyrin−Ferrocene(s): Design, Syntheses, Electrochemistry, and Photochemistry, J. Phys. Chem. B, 108, 31, 11333-11343, 2004.

[7] J. B. Beck, S. J. Rowan, Multistimuli, Multiresponsive Metallo-Supramolecular Polymers, J. Am. Chem. Soc. 125, 46, 13922-13923, 2003.

[8] S. Lim, H. Kim, N. Selvapalam, K-J. Kim, S. J. Cho, G. Seo, K. Kim, Cucurbit[6]uril: Organic Molecular Porous Material with Permanent Porosity, Exceptional Stability, and Acetylene Sorption Properties, Angew Chem Int Ed Engl. ;47(18):3352-5, 2008.

[9] S. Kiyonaka, K. Sada, I. Yoshimura, S. Shinkai, N. Kato, I. Hamachi, Semi-wet peptide/protein array using supramolecular hydrogel, Natute Materials, vol. 3, 2004.

[10] Y. Bae, S. Sukushima, A. Harada, K. Kataoka, Design of Environment-Sensitive Supramolecular Assemblies for Intracellular Drug Delivery: Polymeric Micelles that are Responsive to Intracellular pH Change, Angewandte Chemie, Vol. 42, Iss. 38, 4640-4643, 2003.

[11] Z. Liu, A. C. Fan, K. Rakhra, S. Sherlock, A. Goodwin, X. Chen, Q. Yang, D. W. Felsher, H. Dai, Supramolecular Stacking of Doxorubicin on Carbon Nanotubes for In Vivo Cancer Therapy, Angewandte Chemie, Vol. 48, Iss. 41, 7668-7672, 2009.

[12] D. Hu, Y. Hu, W. Huang, Q. Zhang, Two-photon induced data storage in hydrogen bonded supramolecular azopolymers, Optics Communications, Vol. 285, Iss. 24, 4941-4945, 2012.

[13] Y. Q. Wen, Y. L. Song, G. Y. Jiang, D. B. Zhao, K. Ding, W. F. Yuan, X. Lin, H. J. Gao, L. Jiang, D. B. Zhu, Crystalline Thin Films Formed by Supramolecular Assembly for Ultrahigh-Density Data Storage, Advanced Materials, Vol. 16, Iss. 22, 2018-2021, 2004.

[14] M. Virkki, O. Tuominen, A. Forni, M. Saccone, P. Metrangolo, G. Resnati, M. Kauranen, A. Priimagi, Halogen bonding enhances nonlinear optical response in poled supramolecular polymers, J. Mater. Chem. C, 3, 3003, 2015.

[15] A. D. Grishina, Y. G. Gorbunova, T. V. Krivenko, L. A. Lapkina, V. V. Savel'ev, A. V. Vannikov, A. Y. Tsivadze, Photorefractive and Nonlinear Optical Properties of Indium(III)Tetra(15-Crown-5)Phthalocyaninate-Based Composites, Protection of Metals and Physical Chemistry of Surfaces, Vol. 50, No. 4, pp. 472–479, 2014.

[16] L. Dordević, T. Marangoni, F. De Leo, I. Papagiannouli, P. Aloukos, S. Couris, E. Pavoni, F. Monti, N. Armaroli, M. Prato, D. Bonifazi, [60]Fullerene-poryphyrin [n]pseudorotaxanes: self-assembly, photophysics and third-order NLO response, Phys. Chem. Chem. Phys., 18, 11858, 2016.

[17] A. Aditya Prasad, S. Kalainathan, S. P. Meenakshisundaram, Supramolecular architecture of third-order nonlinear optical picrate: Crystal growth and DFT approach, Optik 127, 6134–6149, 2016.

[18] Z. Zheng, Z-P Yu, M-D Yang, F. Jin, L-N Ye, M. Fang, H-P Zhou, J-Y Wua, Y-P Tiana, Silver(I) supramolecular complexes generated from isophorone-based ligands: crystal structures and enhanced nonlinear optical properties through metal complexation, Dalton Trans., 43, 1139, 2014.

[19] H-Y Bie, J-H Yu, J-Q Xu, J. Lu, Y. Li, X-B Cui, X. Zhang, Y-H Sun, L-Y Pan, Synthesis, structure and non-linear optical property of a copper(II)thiocyanate three-dimensional supramolecular compound, Journal of Molecular Structure 660, 107–112, 2003.

[20] X. Tong, J. Xiang, F. Shi, Y. Zhao, Near-Infrared Light-Sensitive Supramolecular Gel with Enhanced Visible Light Upconversion, Adv. Optical Mater., 4, 1392–1396, 2016.

[21] G. I. Pascu, A.C. G. Hotze, C. Sanchez-Cano, B. M. Kariuki, M. J. Hannon, Dinuclear Ruthenium(II) TripleStranded Helicates: Luminescent Supramolecular Cylinders That Bind and Coil DNA and Exhibit Activity against Cancer Cell Lines, Angewandte Chemie, Vol 46, 23, 4374-4378, 2007.

[22] A. Zawadzka, P. Płóciennik, J. Strzelecki, A. Korcala, A. K. Arof, B. Sahraoui, Impact of annealing process on stacking orientations and second order nonlinear optical properties of metallophthalocyanine thin films and nanostructures, Dyes And Pigments, Volume: 101 Pages: 212-220, 2014.

[23] A. Zawadzka, A.Karakas, P. Płóciennik, J. Szatkowski, Z. Łukasiak, A. Kapceoglu, Y. Ceylan, B. Sahraoui, Optical and structural characterization of thin films containing metallophthalocyanine chlorides, Dyes And Pigments, Volume: 112, Pages: 116-126, 2015.

[24] P. Sutar, V.M. Suresh, T.K. Maji, Tunable emission in lanthanide coordination polymer gels based on a rationally designed blue emissive gelator, Chem. Commun. 51, 9876-9879, 2015.

[25] D. D. Diaz, D. Kuhbeck, R. J. Koopmans, Stimuli-responsive gels as reaction vessels and reusable catalysts, Chem. Soc. Rev. 40, 427-448, 2011.

[26] T. Vermonden, R. Censi, W.E. Hennink, Hydrogels for Protein Delivery Chem. Rev. 112, 2853-2888, 2012.

[27] S. Zhang, M.A. Greenfield, A. Mata, L. C. Palmer, R. Bitton, J. R. Mantei, C. Aparicio, M.O. de La Cruz, S.I . Stupp, A self-assembly pathway to aligned monodomain gels, Nat. Mater. 9,594-601, 2010.

[28] N. G. White, A Rapid and Straightforward Supramolecular Self-Assembly Experiment To Prepare and Characterize a Triple Helicate Complex, Journal of Chemical Education 2018 95 (4), 648-651

[29] D. Laskowski, J. Strzelecki, K. Pawlak, H. Dahm, A,.Balter, Efect of ampicillin on adhesive properties of bacteria examined by atomic force microscopy. Micron 112, 84–90 (2018).

[30] B. Kulyk B, A. P. Kerasidou, L. Soumahoro, C. Moussallem, F. Gohier, P. Frère, B. Sahraoui, Optimization and diagnostic of nonlinear optical features of π-conjugated benzodifuran-based derivatives. RSC Adv 6:14439-14447, 2016.

[31] A. Zawadzka, K. Waszkowska, A. Karakas, P. Płóciennik, A. Korcala, K. Wisniewski, M. Karakaya, B. Sahraoui, Diagnostic and control of linear and nonlinear optical effects in selected self-assembled metallophthalocyanine chlorides nanostructures. Dyes Pig., Vol. 157, 151-162, 2018.

[32] A. Zawadzka, P. Płóciennik, J. Strzelecki, M. Pranaitis, S. Dabos-Seignon, B. Sahraoui, Structural and nonlinear optical properties of as-grown and annealed metallophthalocyanine thin films, Thin Solid Films 545, 429–437, 2013.

[33] B. Sahraoui, J. Luc, A. Meghea, R. Czaplicki, J-L Fillaut, A. Migalska-Zalas, Nonlinear optics and surface relief gratings in alkynyl-ruthenium complexes, J. Opt. A, Pure Appl. Opt. 11, 2009.

[34] B. Kulyk, D. Guichaoua, A. Ayadi, A. El-Ghayoury, B. Sahraoui, Metal-induced efficient enhancement of nonlinear optical response in conjugated azo-based iminopyridine complexes, Organic Electronics 36, 1-6, 2016.

[35] G. J. Lee, S. W. Cha, S. J. Jeon, J. –I. Jin, J.S. Yoon, Second-order nonlinear optical properties of unpoled bent molecules in powder and in vacuum-deposited film, Journal of the Korean Physical Society, 39(5), 912-915, 2001.

[36] S.K. Kurtz, J. Jerphagnon, M.M. Choy, Numerical Data and Functional Relationships in Science and Technology, New Series, Group III: Crystal and Solid State Physics, Landolt-Bornstein New Ser. 11, 671, 1979.

[37] K. Kubodera, H. Kobayashi, Determination of Third-Order Nonlinear Optical Susceptibilities for Organic Materials by Third-Harmonic Generation, Molecular Crystals and Liquid Crystals Incorporating Nonlinear Optics, 182:1, 103-113, 1990.

[38] F. Kajzar, Y. Okada-Shudo, C. Merrit, Z. Kafafi, Second- and third-order non-linear optical properties of multilayered structures and composites of C60 with electron donors, Synth. Met. 117, 2001.

[39] S. K. Vellas, J. E. M. Lewis, M. Shankar, A. Sagatova, J. D. A. Tyndall, B. C. Monk, C. M. Fitchett, L. R. Hanton, J. D. Crowley, [Fe2L3]4+ Cylinders Derived from Bis(bidentate) 2-Pyridyl-1,2,3-triazole “Click” Ligands: Synthesis, Structures and Exploration of Biological Activity, Molecules 2013, 18, 6383-6407

[40] S. E. Howson, L. E. N. Allan, N. P. Chmel, G. J. Clarkson, R. van Gorkum, P. Scott, Self-assembling optically pure Fe(A–B)3 chelates, Chem. Commun., 13, 2009, 1727–1729

[41] A. Zawadzka, P. Płóciennik, A. Korcala, P. Szroeder, Optical properties of chiral single-walled carbon nanotubes thin films, Opt, Mater. vol 96 (2019) 109295

[42] B. Kulyk, K. Waszkowska, A. Busseau, C. Villegas, P. Hudhomme, S. Dabos-Seignon, A. Zawadzka, S. Legoupy, B. Sahraoui, Penta(zinc porphyrin)[60]fullerenes: Strong reverse saturable absorption for optical limiting applications, Applied Surface Science 533 (2020) 147468

[43] B. Kulyk, D. Guichaoua, A. Ayadi, A. El-Ghayoury, B. Sahraoui, Functionalized azo-based iminopyridine rhenium complexes for nonlinear optical performance, Dyes and Pigments 145 (2017) 256-262

[44] L. Pálfalvi, B. C. Tóth, G. Almási, J. A. Fülöp & J. Hebling, A general Z-scan theory, Appl. Phys. B 97, 679, 2009.

[45] E. W. Van Stryland and M. Sheik-Bahae, Z-scan Measurements of Optical Nonlinearities in Characterization Techniques and Tabulations for Organic Nonlinear Materials, ed. M. G.

Kuzyk and C. W. Dirk, Marcel Dekker, Inc., 1998, p. 655.

[46] K. Iliopoulos, D. Potamianos, E. Kakkava, P. Aloukos, I. Orfanos, and S. Couris, Ultrafast third order nonlinearities of organic solvents, Optics Express Vol. 23, Issue 19, pp. 24171-24176, 2015.

[47] R. del Coso and J. Solis, Relation between nonlinear refractive index and third-order susceptibility in absorbing media, Journal of the Optical Society of America B Vol. 21, Issue 3, pp. 640-644, 2004.

[48] G. I. Stegeman and R. A. Stegeman, Nonlinear optics: phenomena, materials, and devices, Wiley, Hoboken, 2012.

[49] Guo Dong, Pang Ke-liang, Duan Chun-ying, He Cheng, and Meng Qing-jin, Design and Crystal Structures of Triple Helicates with Crystallographic Idealized D3 Symmetry: The Role of Side Chain Effect on Crystal Packing, Inorganic Chemistry 2002 41 (23), 5978-5985 DOI: 10.1021/ic0203623

[50] Gaussian 09, Revision D.01, Gaussian, Inc., Wallingford CT, 2009

[51] J. Moellmann and S. Grimme, Dispersion-Corrected Density Functional Theory for Aromatic Interactions in Complex Systems, Acc. Chem. Res. 46, 4, 916–926, 2013.

[52] M. S. Gordon, M.W. Schmidt, Advances in electronic structure theory: GAMESS a Decade Later, C. E. Dykstra, G. Frenking, K.S. Kim, G.E. Scuseria, (eds.), in: Theory and Applications of Computational Chemistry: the first forty years, Elsevier, Amsterdam, 2005, 1167-1189.

[53] F. Kajzar, Y. Okada-Shudo, C. Meritt and Z. Kafafi, Second- and third-order non-linear optical properties of multi-layered structures and composites of C60 with electron donors, Synth. Met., 117 (2001) 189-193.

[54] M. Ferrero, Bartolomeo Civalleri, M. Rérat, R. Orlando, R. Dovesi, The calculation of the static first and second susceptibilities of crystalline urea: A comparison of Hartree–Fock and density functional theory results obtained with the periodic coupled perturbed Hartree–Fock/Kohn–Sham scheme “, J. Chem. Phys. 131 (2009) 214704).

[55] Cojan, C.; Agrawal, G.P.; Flytzanis, C. Optical properties of one-dimensional semiconductors and conjugated polymers. Physical Review B 1977, 15, 909–925.

[56] W. Leupacher and A. Penzkofer, “Third-Order Nonlinear Susceptibilities of Dye Solutions Determined by Third-Harmonic Generation”, Appl. Phys. B 36, 25-31, 1985.